JOURNAL OF CHEMICAL INFORMATION AND MODELING

Article

pubs.acs.org/jcim

Antioxidant Efficiency of Oxovitisin, a New Class of Red Wine Pyranoanthocyanins, Revealed through Quantum Mechanical Investigations

Stefano Alcaro,[†] Sandro Giuseppe Chiodo,*[,†] Monica Leopoldini,[‡] and Francesco Ortuso[†]

[†]Dipartimento di Scienze della Salute, Università degli Studi "Magna Græcia" di Catanzaro, Campus Universitario "S. Venuta", Viale Europa, 88100 Catanzaro, Italy

[‡]Istituto Tecnico Industriale "Galileo Galilei", Via Dino Menci 1, 52100 Arezzo, Italy

ABSTRACT: Oxovitisin is a natural antioxidant present in aged wine and comes from the chemical transformation undergone by anthocyanins and pyranoanthocyanins. Its antioxidant radical scavenging capacity was theoretically explored by density functional theory (DFT)/B3LYP methods. The O−H bond dissociation energy (BDE), the ionization potential (IP), the proton affinity (PA), and the metal−oxovitisin binding energy (BE) parameters were computed in the gas-phase and in water and benzene solutions. Results provided molecular insight into factors that influence radical scavenging potential of this new class of anthocyanins.

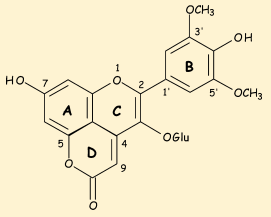

INTRODUCTION

Phenolic compounds are plant secondary metabolites that are commonly present in herbs and fruits such as berries, apples, citrus fruit, grapes, vegetables like onions, olives, tomatoes, broccoli, lettuce, soybeans, grains and cereals, green and black tea, coffee beans, propolis, and red and white wine.[1−9]

They attracted growing global interest upon the discovery of the so-called "French Paradox", i.e. the observation that although the French have smoking tendency and a diet rich in fats, they show much reduced rates of coronary heart diseases when compared with northern European nations such as the UK and Germany.[10] The most popular explanation for these findings is recognized in the relatively high daily consumption by the French of red wine rich in phenolic compounds which in some way act to protect them from heart diseases.[11,12]

All phenolic compounds possess an aromatic ring bearing at least one hydroxyl substituent. A further classification divides them in simple phenols and polyphenols,[13,14] possessing at least two phenol subunits, and including the flavonoids, the stilbenes, and those compounds having three or more phenol subunits (hydrolyzable and nonhydrolyzable tannins).[14] The basic structural feature of flavonoids is the flavan (2-phenyl-benzo-γ-pyran) nucleus, a system of two benzene rings (A and B) linked by an oxygen-containing pyran ring (C) (Figure 1).

Anthocyanins belong to the flavonoids group and are responsible for the red and blue colors of plant organs such as fruits, flowers, and leaves.[15]

Anthocyanins are believed to act as antioxidants,[16] but they have also been proposed to have other biological activities that produce beneficial effects on human health,[17−20] including inhibition of cancer cell growth in vitro,[21] induction of insulin production in isolated pancreatic cells,[22] suppression of inflammatory processes,[20] protection against age-related declines in cognitive behavior and neuronal dysfunction in the central nervous system.[23]

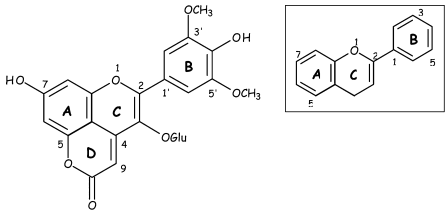

Figure 1. Structures of oxovitisin (in the box, basic representation of flavonoids).

Anthocyanins are responsible for the color of red wine since they are extracted from grape berries during the wine-making process.

During the aging in wood and storage in bottles, wine undergoes many different changes. One of the altered parameters during aging is the color, which is a very important sensory characteristic of red wine.[24] Anthocyanins seem to determine the color of red wine since they are converted, through chemical transformations during wine aging, to new pigments that become responsible for the changing color and the longevity of wine.[25]

The new pigments formed have been first thought to result mainly from condensation reactions between anthocyanins and flavanols directly or mediated by acetaldehyde.[26−32] Nevertheless, over the past decade, reactions involving anthocyanins with other compounds such as pyruvic acid,[33−38] vinylphenol,[39,40] vinylcatechol,[41] α-ketoglutaric acid,[42] acetone,[42−44] and 4-vinylguaiacol[44] have been demonstrated to yield to new families of anthocyanin-derived pigments, namely pyranoanthocyanins, with spectroscopic features that may somehow contribute to a more orange-red color. Normally the pyranoanthocyanin structure can be formed through the

Received: July 28, 2012
Published: January 4, 2013

reaction of an anthocyanin molecule with a compound containing a polarizable double bond.[45] Thus, compared to the free anthocyanins, pyranoanthocyanins have two heteroaromatic rings, and they have a dynamic equilibrium among different flavylium cation forms. These new pigments are mainly formed from grape anthocyanins during the fermentation of must and later during the maturation and aging of red wines.[46,47]

Pyranoanthocyanins have been identified from red wines, especially in the aged red wines, including carboxy-pyranoanthocyanins (A type vitisins), B type vitisins, methylpyranoanthocyanins, hydroxyphenyl-pyranoanthocyanins (pinotins), flavanyl pyranoanthocyanin, and their second generated pigments, such as flavanyl/phenyl vinylpyranoanthocyanins (portisins), pyranone-anthocyanins (oxovitisins), pyranoanthocyanin dimers, and others.[46,48]

Oxovitisins (pyranone-anthocyanin) (Figure 1) display only a pronounced broad band around 370 nm in the UV−vis spectrum and therefore contribute yellow color to a wine. They are generally direct derivatives of carboxypyranoanthocyanins, especially vitisin A. In their formation, a water molecule first attacks the positively charged C10 position of the pyranoanthocyanin precursor, leading to their hemiacetal formation. The resulting intermediates undergo a series of decarboxylation, oxidation, and dehydration reactions, producing the final new and neutral pyran-2-one structures, as shown in Scheme 1.[49]

Scheme 1. Mechanism of Formation of Oxovitisins from Carboxy-pyranoanthocyanins

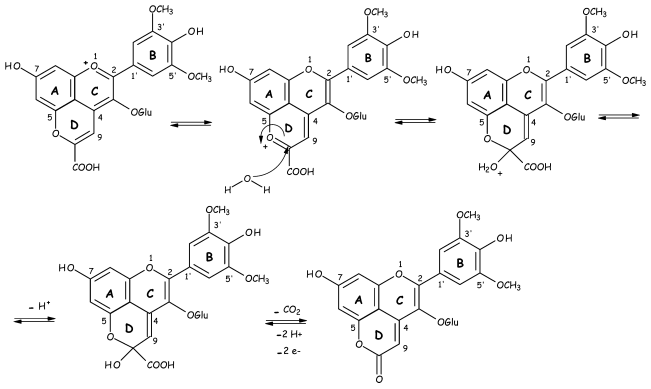

The molecular basis for the antioxidant properties of polyphenols and thus of anthocyanins is revealed into three main mechanisms, arising from the reaction with free radicals[50−53] and from the chelation of metals.[54] Moreover similar scaffolds, like quercetin, have been also reported for the ability to bind selectively the isoform A of monoamine oxidases by theoretical and experimental methods.[55]

As primary antioxidants, polyphenols inactivate free radicals according to the hydrogen atom transfer (1) and the single electron transfer (2) mechanisms. In mechanism 1, the antioxidant (ArOH) reacts with the free radical (R·) by transferring to it a hydrogen atom.

$$\mathrm{ArOH} + \mathrm{R}\cdot \rightarrow \mathrm{ArO}\cdot + \mathrm{RH} \quad (1)$$

The products of the reaction are the harmless RH species and the oxidized ArO· radical. ArO· is much less reactive regarding R· because it is usually stabilized by several factors.[50−54]

The single electron transfer mechanism (2) provides an electron to be donated to the R·:

$$\mathrm{ArOH} + \mathrm{R}\cdot \rightarrow \mathrm{ArOH}^{+}\cdot + \mathrm{R}^{-} \quad (2)$$

The anion R^- is an energetically stable species with an even number of electrons, whereas the cation radical $ArOH^{+}\cdot$ is also in this case a less reactive radical species.

The studies on mechanism of chelation of transition metal cations such as iron,[54] lead,[56] aluminum,[57] and copper[58] have shown that flavonoids may represent good chelating agents.

Most of flavonoids are believed to act through the H-atom transfer since higher energies are involved in the one-electron transfer process.[50]

In the past decade, many computational studies have been devoted to the elucidation of phenolics and flavonoids antioxidant activity. Particularly, several density functional theory (DFT) investigations concerning the determination of the bond dissociation energy (BDE) of phenolic OH groups and the ionization potential (IP)[50−53] have given considerable information about antioxidant ability since the lower the BDE and IP values, the more favorite the hydrogen abstraction and the electron transfer reactions. The gas phase values of BDE and IP computed for flavonoids usually fall in a range of 70−90 and 160−190 kcal/mol, respectively. Other studies concerning the computation of the metal−phenolic binding energy (BE) have indicated that these compounds are effective in sequestering transition metals in such a way to prevent their involvement in the Fenton reaction. DFT/B3LYP investigation on some pyranoanthocyanins has revealed them to be more powerful antioxidants than anthocyanins.

The main aim of this study is to determine the geometrical and electronic features of the oxovitisin type molecule and of its radical species formed upon hydrogen/electron removal, as well as of the iron(II)−oxovitisin complexes. To corroborate the antioxidant capability within the working mechanisms proposed in the literature, the BDE, IP, proton affinity (PA), and BE thermodynamic parameters have been computed as the more representative descriptors for the radicals scavenging ability.

METHODS

All structures of oxovitisin and its radicals and anions, and of the iron complexes, were optimized without constraints, using tight convergence criteria, employing the DFT/B3LYP (UB3LYP for the resulting radicals) exchange-correlation functional and the 6-311++G** basis set for C, O, and H atoms,[59] and, to save computer time, the LACV3P++** basis set for Fe atom, coupled with an effective core potential for the core electrons, was used in all calculations concerning the complex species. These basis sets are implemented in the Jaguar V9.7 computational programs suite.[60]

Starting geometries of the protonated oxovitisin and of its iron complexes were generated coupling Monte Carlo (MC) conformational search included in MacroModel V9.8[61,62] and cluster analysis. In detail, 100 000 structures were automatically generated by random rotation of the available single bonds. Metal relative position was also investigated allowing free movement within 15 Å around the oxovitisin. In order to eliminate duplicated conformation, each structure was geometrically compared to the others and discarded if the root mean squared deviation (RMSd), computed onto the not hydrogen atoms, was lower than 0.05 Å. Each MC conformer was energy optimized using the OPLS-2005 force field[63] and solvent effects were taken into account by means of the GB/

dx.doi.org/10.1021/ci300354s | J. Chem. Inf. Model. 2013, 53, 66−75

SA[64] water implicit solvation model. The final MC ensemble was submitted to Boltzman population analysis. Complexes were submitted to clustering.[65] Most stable conformation of the oxovisitin and the representative structure of top three stable clusters was adopted as starting geometry for the complexes at each putative site. Oxovisitin anion models were derived from the previously reported removing the corresponding proton.

Vibrational frequencies were obtained at the same level of theory, with the aim to characterize all structures as minima and to estimate zero point energy corrections that were included only into the gas-phase energy contributions.

The unrestricted open-shell approach was used for radical species.

Solvent effects were computed over gas phase equilibrium geometries by the standard Poisson−Boltzmann (PB) solver,[66,67] implemented in the Jaguar V9.7 program package.[60] This model was used for the parent molecules and its derivatives. The dielectric constants of 80.37 and of 2.284 were used to reproduce the water and benzene media, respectively.

The OH bond dissociation energy (BDE) and ionization potential (IP) values were computed as the sum of the energy of the radical resulting from the hydrogen atom abstraction and that of the hydrogen atom minus the energy of the parent molecule, and as the energy difference between the radical cation and the parent molecule, respectively. The proton affinity (PA) is computed as the difference in energy between the anion (A^-) and its neutral species (HA). The iron−oxovitisin binding energy (BE) values were obtained as the difference in energy between the metal complex and the free reactants. The charge transfer effect was analyzed in order to characterize the bonds in these systems by means of the natural bond orbitals (NBOs) technique.[68]

Finally, measures of aromaticity were carried out separately for each ring of the radicals, the anionic species, and the parent molecule. For this purpose, aromaticity indices were obtained applying the harmonic oscillator model of aromaticity (HOMA).[69] In this work, the R_{opt} and α parameters were derived at the above-described level of theory for CC and CO bonds: $R_{opt,CC}$ = 1.395 Å, $R_{opt,CO}$ = 1.281 Å, α_{CC} = 88.60, and α_{CO} = 74.82.

RESULTS AND DISCUSSION

Oxovitisin Radical and Anion Forms. The HOMA analysis was performed over the A, B, C, and D rings of the oxovitisin and its derivatives. The corresponding index values were obtained taking into account the bond distances shown for each ring in Scheme 2. Their relative values are collected in Table 1. The B3LYP computation finds as minimum structure for oxovitisin (Figure 2) the conformation exhibiting a π electron delocalization and conjugation involving the rings A, C, and D, and a H-bond in the ring B established between the 4′OH and the 3′-OCH_3 group (2.090 Å). A further H-bond is established between the carbonyl oxygen and the sugar C_6OH

Scheme 2. Representation of Bond Distances of the A, B, C, and D Rings Considered in the HOMA Analysis

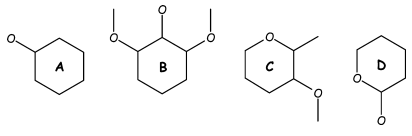

Table 1. HOMA Index Values for A, B, C, and D Rings of the Oxovitisin and Its Derivatives

	A	B	C	D
oxovitisin	0.928	0.592	0.493	0.673
radical 4′OH	0.929	0.490	0.504	0.689
radical 7OH	0.863	0.593	0.490	0.728
radical cation	0.945	0.591	0.566	0.666
anion 4′OH	0.911	0.479	0.575	0.633
anion 7OH	0.865	0.574	0.461	0.803

at 2.610 Å. Ring B appears to be slightly implicated in the whole electron π delocalization, as the HOMA index value of 0.592 reported in Table 1 and the $C_3-C_2-C_{1'}-C_{2'}$ dihedral (Ψ_1) value of 146.1° indicate. In fact, the corresponding value computed in this work for the 2,6-dimethoxyphenol is slightly lower, 0.585. Calculations predict a nonplanar structure for oxovitisin as encountered for pyranoanthocyanins recently.[70]

As far as the energetic properties as BDE, IP, and PA are concerned, it is very unlikely that the glucoside moiety attached to the C_3 position in ring C may have some influence, since the reactive site is generally accepted to be the flavonoid part,[50] so H-atom and H^+ abstraction will be not examined for the alcoholic groups in the sugar residue. The chelating ability instead could be affected by the sugar ring so alcoholic groups will be included in the computations, as discussed later.

By abstracting a hydrogen atom from the two hydroxyl groups present on the oxovitisin molecule, two radical species are obtained, whose optimized geometries are reported in Figure 2.

Radical 4′OH, arising from the abstraction of a hydrogen atom from the OH group attached at the 4′ carbon, is more stable than the 7OH by 4.9 kcal/mol (values in Table 2). This difference in energy can be explained by considering that in the 4′OH radical species, apart from the possibility of resonance effects, the electronic vacancy generated on the radical formation center is stabilized by hyperconjugation with the adjacent 3′ and 5′ methyl groups. For this species, the HOMA index of the ring B is affected by the presence of the unpaired electron that seems to reduce the conjugation on this ring. In fact, with respect to the parent molecule, this value decreases from 0.592 to 0.490.

The stability of the 7OH radical arises from the possibility of resonance effects between rings A, C, and D. Particularly, conjugation appears to decrease in the ring A (HOMA index changes from 0.928 for the oxovitisin to 0.863 for the radical 4′OH) and to increase on ring D (HOMA index is computed to be 0.673 and 0.728, in the oxovitisin and in the radical, respectively).

For both radicals, the H-bond involving the carbonyl oxygen and the sugar C_6OH is retained (2.437 and 2.505 Å, for the 4′OH and 7OH).

The plotting of spin density in these species (Figure 3) indicates that in both cases the odd electron remains on the radicalized oxygen atom.

The radical energetic gap in the condensed phase is found to be 1.7 kcal/mol in water and 3.8 kcal/mol in benzene media, being again the 4′OH species the minimum. Thus, solvation seems to decrease the energy separation between the two species, especially in the water solution.

Radical cation species arising from the abstraction of one electron from the HOMO of oxovitisin retains the H-bond in the ring B (2.086 Å) like in the parent molecule, but gaining in

dx.doi.org/10.1021/ci300354s | J. Chem. Inf. Model. 2013, 53, 66−75

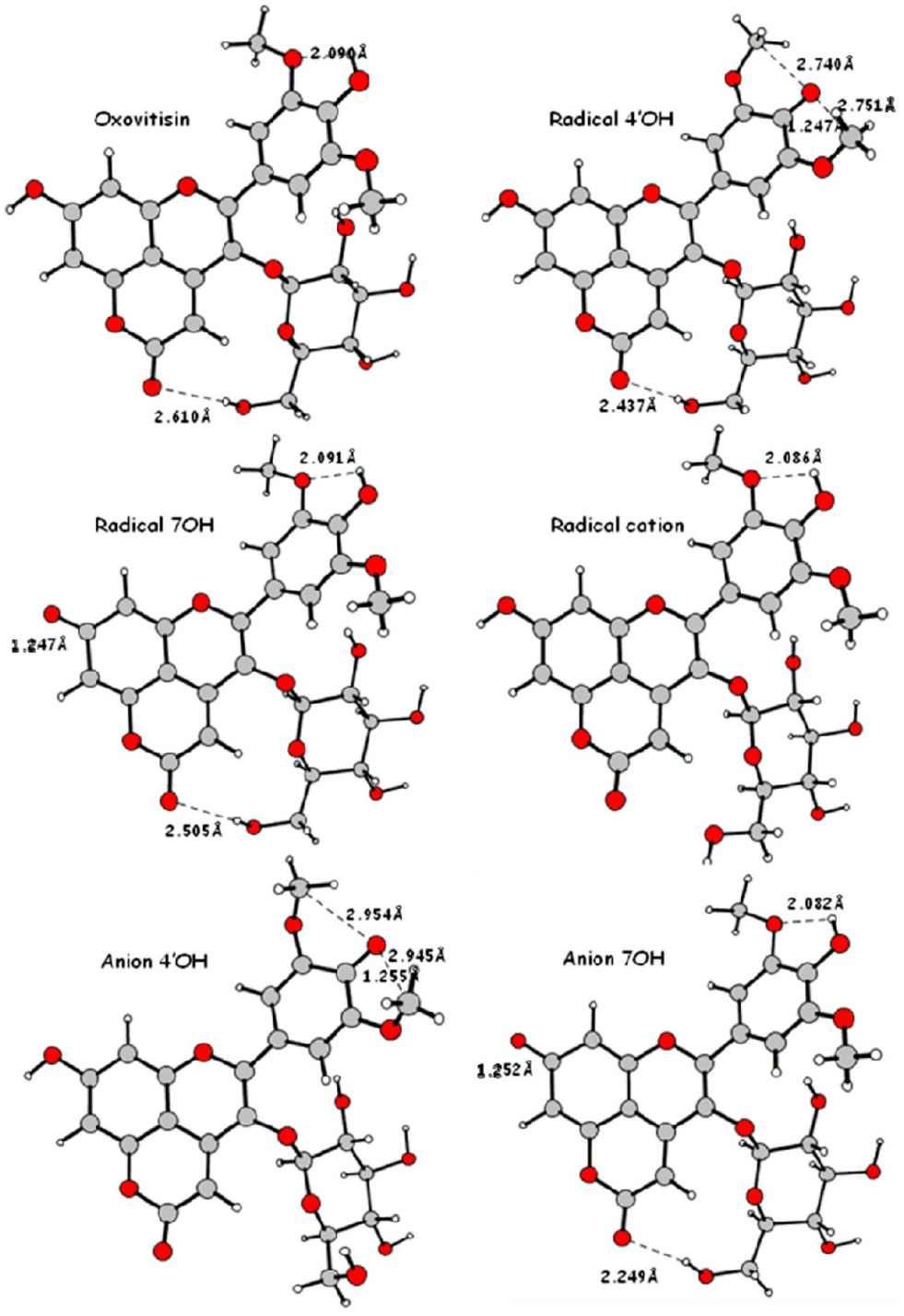

Figure 2. B3LYP minimized geometries of oxovitisin and its derivatives.

Table 2. Relative Energies ΔE (kcal/mol) of Radical and Anionic Species of Oxovitisin

	ΔE (gas)	ΔE (water)	ΔE (benzene)
radical 4′OH	0.0	0.0	0.0
radical 7OH	4.9	1.7	3.8
anion 4′OH	0.0	13.0	1.7
anion 7OH	3.7	0.0	0.0

planarity ($C_3-C_2-C_{1'}-C_{2'}$ dihedral Ψ_1 is 157.8°) (Figure 2). For this species, the atomic spin density reported in Figure 2 shows that the unpaired electron is located mostly on carbons in the rings C and D. HOMA indices in Table 1 indicate a major π conjugation on rings A and C of 0.945 and 0.566, respectively. The OH BDE and the IP computed for oxovitisin in the gas and condensed phases are collected in Table 3.

Gas-phase BDE is computed to be 78.2 and 83.1 kcal/mol, as far as the 4′OH and 7OH groups are concerned. The lower value for the hydroxyl in the ring B (4′OH) is determined by the possibility of hyperconjugation between methyl groups and radicalized oxygen in this radical species that helps in stabilizing the electronic vacancy. The corresponding values in water and benzene media are 94.5 and 90.5, and 96.1 and 94.3 kcal/mol,

dx.doi.org/10.1021/ci300354s | J. Chem. Inf. Model. 2013, 53, 66−75

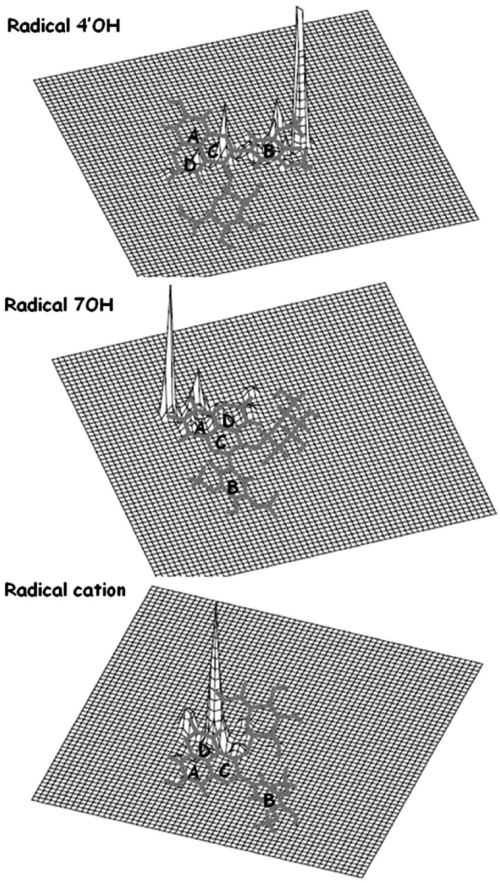

Figure 3. Atomic spin density distribution in oxovitisin radical species.

Table 3. BDE, IP, and PA (kcal/mol) for Oxovitisin

	BDE (gas)	BDE (water)	BDE (benzene)
4′OH	78.2	94.5	90.5
7OH	83.1	96.1	94.3
	IP (gas)	**IP (water)**	**IP (benzene)**
	162.5	132.9	146.0
	PA (gas)	**PA (water)**	**PA (benzene)**
4′OH	317.6	296.2	310.2
7OH	321.3	283.2	308.5

considering the 4′OH and the 7OH groups, in order. Corrections in solution cause an increase of these values by around 13−16 kcal/mol in the water and 11−12 kcal/mol in the benzene media. Water and benzene solvents appear to have similar effects on BDE probably because of the affinity shown by oxovitisin, like other flavonoids, for both polar and nonpolar environments.

The BDE value of oxovitisin is similar to the one of vitisin A reported in the literature (81.7 kcal/mol, value in the gas phase),[70] from which oxovitisin comes, thus indicating that the BDE in pyranoanthocyanins is affected primarily by the arrangement of the hydroxyl in the ring B.

IP values (Table 3) are 162.5, 132.9, and 146.0 kcal/mol, in vacuo and in water and benzene media, respectively, indicating that oxovitisin is a good candidate to work within the electron transfer mechanism. Corrections in solution cause a decrease of these values by around 30 and 17 kcal/mol in the water and benzene media, probably through a better stabilization of the positively charged species formed. IP values for vitisin A available in the literature are 230.1 (gas-phase), 137.7 (water), and 179.8 (benzene) kcal/mol,[70] that are higher compared to oxovitisin. The absence of the positive charge in the parent molecule and the also the presence of the carbonyl group in the ring D seem to decidedly lower the energy required to abstract the electron from the HOMO of the molecule with respect to vitisin A. So oxovitisin appears to be a better radical scavenger than vitisin A, as far as the single electron transfer mechanism is concerned.

Deprotonated forms of oxovitisin arise from the oxovitisin → oxovitisin$^-$ + H$^+$ reaction scheme. Deprotonation may occur at the 4′OH and 7OH site, thus generating two anions whose optimized geometries are reported in Figure 2.

The 4′OH anion shows geometrical features similar to the semiquinone form coming from the hydrogen atom abstraction process. The $C_{4'}$—O distance decreases from 1.352 in the parent molecule to 1.255 Å in the anion, thus underlining that a C═O double bond is formed and that the excess of negative charge arising from proton abstraction is distributed over the rings B and C (in the latter, conjugation increases as the value of 0.575 of the HOMA index for the anion 4′OH suggests), also thanks to a better planar arrangement (C_3—C_2—$C_{1'}$—$C_{2'}$ dihedral Ψ_1 value is 162.7°).

In the 7OH anion also a C═O bond is established at 1.252 Å with the negative charge delocalized on the aromatic rings. Conjugation increases on ring D (HOMA index value is computed 0.803 in the anion, while in the parent is 0.673).

Generated anions show a gas-phase ΔE of 3.7 kcal/mol in favor of the 4′OH anion, as reported in Table 2. Computations in the condensed phase favor the 7OH anion by 13.0 (water solution) and 1.7 (benzene solution) kcal/mol. These findings indicate that the interactions with the methyl groups as found for the semiquinone species have a small effect on the stabilization of the deprotonated forms, whose relative energy seems to depend mainly on the possibility of delocalization of the negative charge originated upon proton abstraction. In the condensed phases, the stabilizing effect for one species rather than another could be due to different dipole solute−dipole solvent interactions.

Proton affinity (values in Table 3) is computed to be 317.6 and 321.3 kcal/mol in vacuo for the 4′OH and 7OH sites, respectively, while in water and benzene media the PA values are 296.2 and 310.2 kcal/mol for the 4′OH species and 283.2 and 308.5 kcal/mol for the 7OH one. Solvents seem to slightly favor the deprotonation process by ∼7−38 kcal/mol.

The PA energetic values computed here are consistent with the values reported in the literature for polyphenols, which fall in a range of 312.5−327.5 kcal/mol.[71] Proton affinities of anthocyanins are usually found to be smaller (cyanidin PA is 237.7 kcal/mol for the 5OH group in the ring A[71]), but this is not surprising because anthocyanins are positive charged forms, so the deprotonation in that case gives rise to very stable neutral species.

The systems for which the acidity values are low can be easily deprotonated in vivo in physiological environment and so they can chelate transition metal cations, inactivating them from giving radical reactions.

Iron Chelation and Oxovitisin−Fe Complexes. Transition metals ions in their low oxidation state, like Fe^{2+} and Cu$^+$, can catalyze reactions that involve formation of free radicals. Polyphenols and thus pyranoanthocyanins may offer several chelating sites, such as multiple hydroxyls and carbonyl groups,

dx.doi.org/10.1021/ci300354s | J. Chem. Inf. Model. 2013, 53, 66−75

giving rise to stable complexes that, entrapping metals, avoid their participation in free radical generation processes.

In principle, there are three possible sites on oxovitisin for the iron(II) chelation: between the hydroxyl and the methoxy groups in the ring B (two positions) and between the oxygen atoms of the ester moiety in the ring D, with the involvement of the OH groups belonging to the sugar residue in all cases (Scheme 3). The coordination to these sites can give rise to three compounds in oxovitisin.

Scheme 3. Possible Binding Sites for Metal Chelation in Oxovitisin

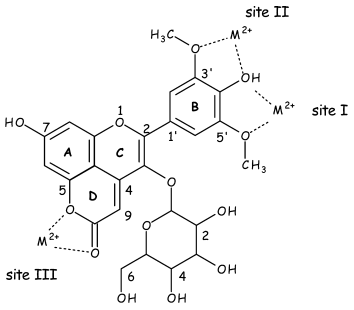

Complex Ia is obtained when Fe^{2+} is coordinated to the oxygen atoms from the $C_{4'}OH$ and the $C_{5'}OCH_3$ groups, at 2.251 and 2.093 Å, respectively. Sugar hydroxyls attached to C_3 and C_4 arranged as to interact with the metal cation at 2.098 and 2.077 Å, respectively (Figure 4). Atomic net charges on the oxygen atoms involved in the iron coordination change from −0.646 to −0.750 |e| for the $C_{4'}O$ and from −0.514 to −0.652 |e| for the $C_{5'}O$, while the charge on iron is computed to be 1.499 |e|.

Complex IIa is characterized by the coordination of iron to the $C_{4'}OH$ ($O-Fe^{2+}$ distance is 2.238 Å), $C_{3'}OCH_3$ ($O-Fe^{2+}$ distance is 2.138 Å) groups, sugar C_3OH ($O-Fe^{2+}$ distance is 2.138 Å), and C_4OH ($O-Fe^{2+}$ distance is 2.083 Å).

Coordination of the metal to the oxygen atoms in the ring D generates the complex IIIa in which Fe^{2+} results to be coordinated to the carbonyl oxygen of the ring D at 1.889 and to the hydroxyl groups of the sugar attached to the C_4 (2.065 Å) and C_6 (2.069 Å). No coordination occurs with the other oxygen in the ring D since the arrangement found ensures to the cation a higher number of coordination.

In all complexes of type *a* the interactions established seem to be prevalently electrostatic with a lesser covalent contribution, as underlined by the atomic net charge found on the cation (1.499, 1.451, and 1.492 |e| for complexes Ia, IIa, and IIIa, respectively).

Ring B seems to be not coplanar with the rest of the molecule, as encountered for free oxovitisin.

The global minimum is the complex IIIa characterized by the monocoordination of the metal to the flavonoid portion. Complexes Ia and IIa are found at 10.2 and 17.4 kcal/mol, respectively. Even if the latter complexes involve a higher coordination number, complex IIIa is energetically favored since in this case iron interacts with the carbonyl oxygen having a better electronic density.

The two OH groups of oxovitisin are slightly acidic, as we have seen previously, so they may exist in some anionic forms at physiological pH values that may be involved in the coordination of the iron metal.

Complex Ib (Figure 4) originates from the coordination of the cation to the deprotonated $C_{4'}O$ and to the $C_{5'}OCH_3$ (iron−oxygen distances are 1.892 and 2.238 Å, respectively) in the 4′OH anion of oxovitisin. Sugar C_3OH and C_4OH oxygen atoms interact with the iron at 2.174 and 2.126 Å, respectively.

Complex IIb is characterized by the interactions of Fe(II) with the deprotonated $C_{4'}O$ and the $C_{3'}OCH_3$, at 1.891 and 2.380 Å, respectively, and with the hydroxyls of the sugar moiety (C_3OH-Fe^{2+} and C_4OH-Fe^{2+} distances are 2.091 and 2.185 Å, in that order).

Complex IIIb proposes a three-coordination of the iron center to the carbonyl oxygen (Fe−O distance is 1.948), C_4OH (Fe−O = 2.197 Å), and C_6OH (Fe−O = 2.137 Å).

Complex Ib is the global minimum, while the other complexes are found at 2.6 (IIb) and 29.8 (IIIb) kcal/mol. The minimum energy structure is obtained when iron coordinates at the deprotonation site. Complex IIb is less favored because of the longer distance with the methoxy.

Interaction of Fe^{2+} with the 7OH anion of oxovitisin entails the formation of four complexes (considering in this case the bonding interaction with the deprotonated C_7O) whose optimized geometries are reported in Figure 4.

In the complexes Ic and IIc the interactions are established between the iron and the oxygen atoms of the ring B ($Fe-OHC_{4'}$ and $Fe-OCH_3C_{5'}$distances are 2.356 and 2.278 Å and $Fe-OHC_{4'}$ and $Fe-OCH_3C_{3'}$ distances are 2.379 and 2.371 Å). In both cases, further interactions are established with the C_3 and C_4 hydroxyl in the sugar molecule (see Figure 4), as encountered for the former complexes of type *a* and *b*.

Complex IIIc is characterized by a Fe^{2+}—O═C distance of 1.913 Å and by C_4OH—Fe^{2+} and C_6OH—Fe^{2+} distances of 2.096 and 2.086 Å, respectively.

Complex IVc shows a $Fe^{2+}-OC_7$ bond distance of 1.879 Å, and C_4OH-Fe^{2+} and C_6OH-Fe^{2+} distances of 2.125 and 2.090 Å, respectively. As Figure 4 shows, in this adduct the coordination of the iron to the sugar causes a certain distortion of the ring C in the oxovitisin as to maximize these interactions.

The global minimum is represented by complex IVc. The other complexes lie at 22.6 (Ic), 25.8 (IIc), and 5.9 (IIIc) kcal/mol. Again, the direct coordination of the cation to the negative charged site entails a good energy stabilization.

As expected, the complexation of oxovitisin and its derived forms by Fe^{2+} cation appears to be a thermodynamically favored process for all complexes examined, as reflected by binding energy (BE) values reported in Table 4. In the case of neutral oxovitisin, the more favorite process is the metal complexation at the carbonyl group in the ring D with a ΔE of −265.2 kcal/mol (complex IIIa).

Complexation of Fe^{2+} on each available site in the 4′OH and 7OH anionic species of oxovitisin entails very important stabilizing energies for the processes. Among the available possibilities, iron prefers to coordinate at the ring B with the OCH_3 group and the deprotonated hydroxyl attached to $C_{4'}$ (complex Ib), with an energy variation associated to this process of −419.3 kcal/mol.

Literature data concerning the ability of flavonoid molecules in chelating transition metals also suggest these compounds to be excellent chelating agents. For example, Fe(II) and Cu(II) complexation energies by quercetin deprotonated species were been computed to be −431.9[54] and −500.2 kcal/mol.[58] Cu(I) and Cu(II) complexation by rooperol shows binding energies of −145.1 and −324.4 kcal/mol.[72]

dx.doi.org/10.1021/ci300354s | J. Chem. Inf. Model. 2013, 53, 66−75

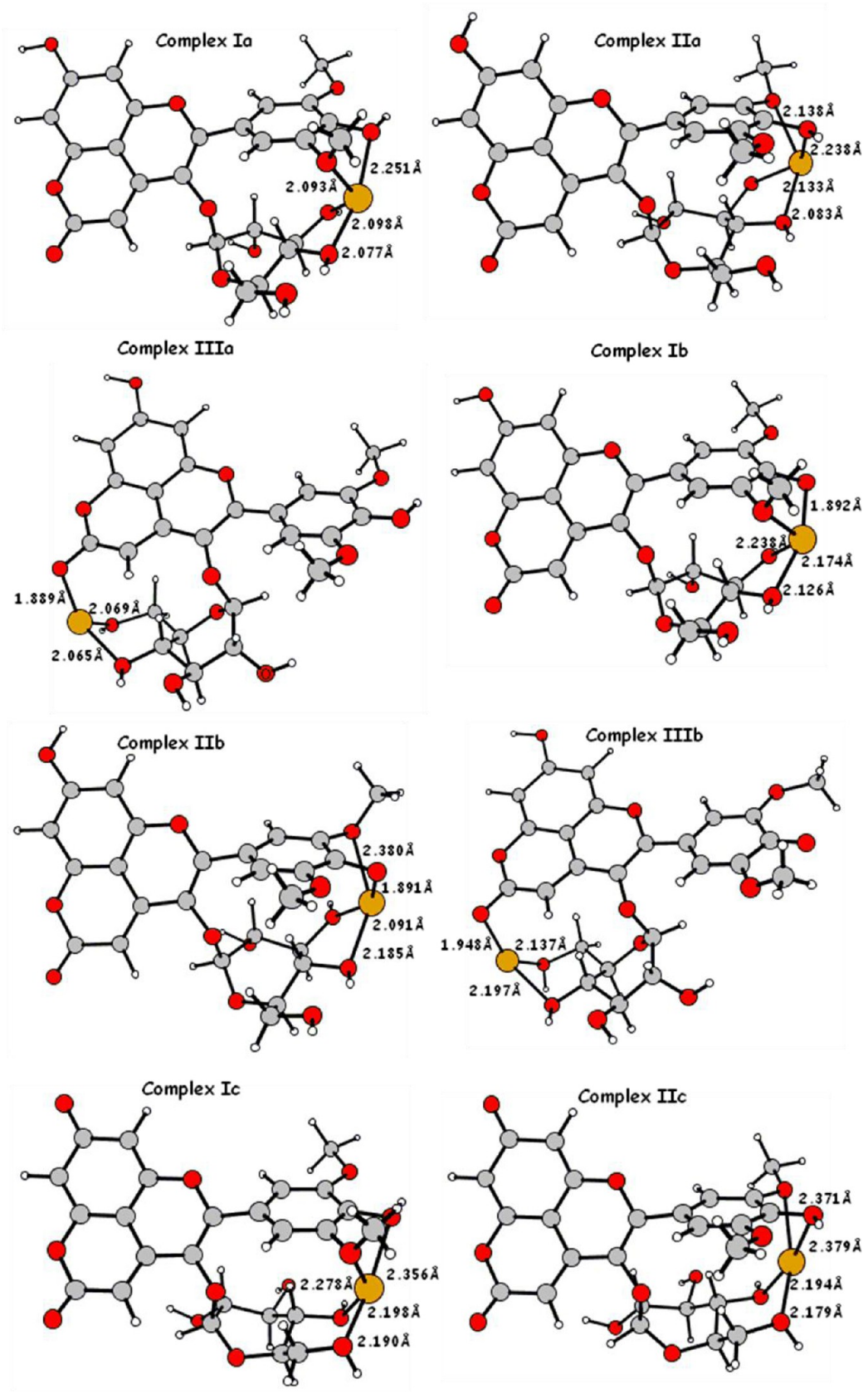

Figure 4. continued

dx.doi.org/10.1021/ci300354s | *J. Chem. Inf. Model.* 2013, 53, 66−75

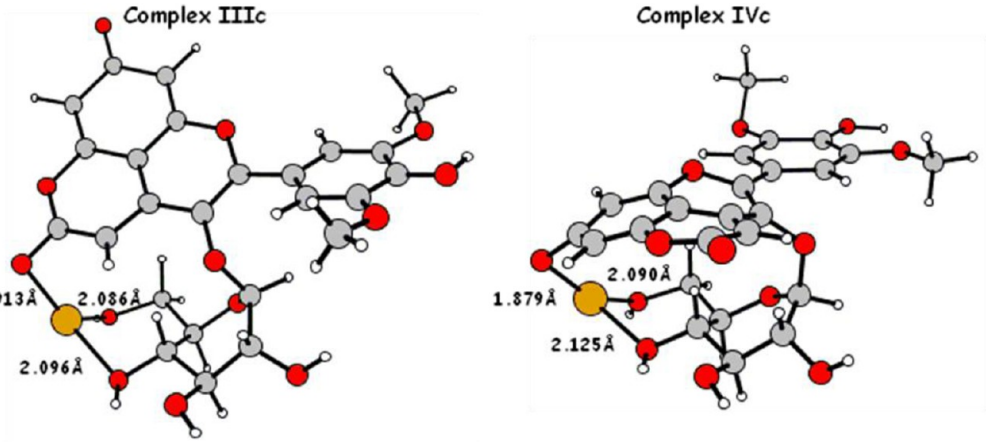

Figure 4. B3LYP minimized geometries of oxovitisin−iron(II) complexes.

Table 4. Binding Energies, BE (kcal/mol) for the Iron(II)−Oxovitisin Complexes

	ΔE	binding energy (BE)
complex Ia	10.2	−255.1
complex IIa	17.4	−247.9
complex IIIa	0.0	−265.2
complex Ib	0.0	−419.3
complex IIb	2.6	−416.8
complex IIIb	29.8	−389.6
complex Ic	22.6	−375.7
complex IIc	25.8	−372.5
complex IIIc	5.9	−392.5
complex IVc	0.0	−398.3

The binding energies associated to the metal complexation suggest that oxovitisin is a good candidate in complexing and thus sequestering iron(II) cation, avoiding it to participate in Fenton chemistry processes.

CONCLUSIONS

We have applied a density functional based method employing the B3LYP functional to the study of a naturally occurring antioxidant compound, oxovitisin. It derives from the chemical transformations undergone by anthocyanins during wine aging, that are responsible for the color, feel, taste, as well as longevity of aged wines.

The main mechanisms proposed in the literature for the antioxidant action of polyphenols as radicals scavengers, consisting in the H-atom and electron transfer, and the metal chelation have been discussed in detail, and structural and electronic features of all oxovitisin species involved in these mechanisms have been determined.

The OH bond dissociation energy (BDE), the adiabatic ionization potential (IP), the proton affinity (PA), and the oxovitisin−iron(II) binding energy (BE) have been computed, since they represent excellent primary indicators of the radical scavenging activity exhibited by these polyphenolic compounds.

Oxovitisin is an aromatic compound, with a high degree of conjugation and delocalization of π electrons. As encountered for pyranoanthocyanins, ring B is not coplanar to the rest of the molecule.

Upon the removal of a hydrogen atom or an electron, radical species originate, in which the odd electron appears to be delocalized as much as possible over the whole molecule. As far as the H atom transfer mechanism is concerned, radicalization occurs preferably on ring B at the $C_{4'}$ position since in this case hyperconjugation phenomena with vicinal $-OCH_3$ become important for the radicals stability.

BDE values are quite similar to those of pyranoanthocyanins, while IP quantities indicate that oxovitisin is a better radical scavenger than vitisin A, as far as the single electron transfer mechanism is concerned.

Iron(II) complexation occurs preferably with the anionic forms of oxovitisin, especially in the ring B, with very favorable reaction energies.

AUTHOR INFORMATION

Corresponding Author

*E-mail: sandro.chiodo@unicz.it.

Notes

The authors declare no competing financial interest.

REFERENCES

(1) Ross, J. A.; Kasum, C. M. Dietary flavonoids: bioavailability, metabolic effects, and safety. *Annu. Rev. Nutr.* **2002**, *22*, 19−34.

(2) Hertog, M. G. L.; Hollman, P. C. H.; Katan, M. B.; Kromhout, D. Intake of potentially anticarcinogenic flavonoids and their determinants in adults in the Netherlands. *Nutr. Cancer* **1993**, *20*, 21−29.

(3) Brit, D. F.; Hendrich, S.; Wang, W. Dietary agents in cancer prevention: flavonoids and isoflavonoids. *Pharmacol. Ther.* **2001**, *90*, 157−177.

(4) Kris-Etherton, P. M.; Hecker, K. D.; Bonanome, A. B.; Coval, S. M.; Binkoski, A. E.; Hilpert, K. F.; Griel, A. E.; Etherton, T. D. Bioactive compounds in foods: their role in the prevention of cardiovascular disease and cancer. *Am. J. Med.* **2002**, *113*, 71−88.

(5) Robak, J.; Gryglewski, R. J. Bioactivity of flavonoids. *Pol. J. Pharmacol.* **1996**, *48*, 555−564.

(6) Rice-Evans, C. A.; Spencer, J. P.; Schroeter, H.; Rechner, A. R. Bioavailability of flavonoids and potential bioactive forms *in vivo*. *Drug Metabol. Drug Interact.* **2000**, *17*, 291−310.

(7) Clifford, M. N. Chlorogenic acids and other cinnamates − nature, occurence and dietary burden. *J. Sci. Food Agric.* **1999**, *79*, 362−372.

(8) Rencher, A. R.; Spencer, P. E.; Kuhnle, G.; Hahn, U.; Rice-Evans, C. A. Novel biomarkers of the metabolism of caffeic acid derivatives *in vivo*. *Free Radic. Biol. Med.* **2001**, *30*, 1213−1222.

(9) Hermann, K. Flavonoid antioxidants in food of plant origin. *XP002133789 & Gordian* **1993**, *93*, 108−111.

(10) Renaud, S.; De Lorgeril, M. Wine, alcohol, platelets, and the French paradox for coronary heart disease. *Lancet* **1992**, *339*, 1523−1526.

(11) Frankel, E. N.; Kanner, J.; German, J. B.; Parks, E.; Kinsella, J. E. Inhibition of oxidation of human low-density lipoprotein by phenolic substances in red wine. *Lancet* **1993**, *341*, 454−457.
(12) Hertog, M. G. L.; Freskens, E. J. M.; Hollman, P. C. H.; Katan, M. B.; Kromhout, D. Dietary antioxidative flavonoids and risk of coronary heart disease: the Zutphen Elderly Study. *Lancet* **1993**, *342*, 1007−1011.
(13) Robbins, R. J. Phenolic acids in foods: an overview of analytical methodology. *J. Agric. Food Chem.* **2003**, *51*, 2866−2887.
(14) King, A.; Young, G. Characteristics and occurrence of phenolic phytochemicals. *J. Am. Diet Assoc.* **1999**, *99*, 213−218.
(15) Strack, D.; Wray, V. Anthocyanins. In *Methods in Plant Biochemistry, Plant Phenolics*; Harborne, J. B., Eds.; Academic Press: London, 1993; Vol. *1*, pp 325−356.
(16) Stinzing, F. C.; Carle, R. Functional properties of anthocyanins and betalins in plants, food, and in human nutrition. *Trends Food Sci. Technol.* **2004**, *15*, 19−38.
(17) Zhang, Y.; Vareed, S. K.; Nair, M. G. Human tumor cell growth inhibition by nontoxic anthocyanidins, the pigments in fruits and vegetables. *Life Sci.* **2005**, *76*, 1465−1472.
(18) Jayaprakasam, B.; Vareed, S. K.; Olson, L. K.; Nair, M. G. Insulin secretion by bioactive anthocyanins and anthocyanidins present in fruits. *J. Agric. Food Chem.* **2005**, *53*, 28−31.
(19) Matsui, T.; Ueda, T.; Oki, T.; Sugita, K.; Terahara, N.; Matsumoto, K. α-Glucosidase inhibitory action of natural acylated anthocyanins. 1. Survey of natural pigments with potent inhibitory activity. *J. Agric. Food Chem.* **2001**, *49*, 1948−1951.
(20) Tall, J. M.; Seeram, N. P.; Zhao, C. S.; Nair, M. G.; Meyer, R. A.; Raja, S. N. Tart cherry anthocyanins suppress inflammation-induced pain behavior in rat. *Behav. Brain Res.* **2004**, *153*, 181−192.
(21) Zhang, Y.; Vareed, S. K.; Nair, M. G. Human tumor cell growth inhibition by nontoxic anthocyanidins, the pigments in fruits and vegetables. *Life Sci.* **2005**, *76*, 1465−1472.
(22) Jayaprakasam, B.; Vareed, S. K.; Olson, L. K.; Nair, M. G. Insulin secretion by bioactive anthocyanins and anthocyanidins present in fruits. *J. Agric. Food Chem.* **2005**, *53*, 28−31.
(23) Joseph, J. A.; Shukitt-Hale, B.; Denisnova, N. A.; Bielinski, D.; Martin, A.; McEwan, J. J.; Bickford, P. C. Reversals of age-related declines in neuronal signal transduction, cognitive, and motor behavioural deficits with blueberry, spinach, or strawberry dietary supplementation. *J. Neurosci.* **1999**, *19*, 8114−8121.
(24) Revilla, I.; González-SanJosé, M. L. Effect of different oak woods on aged wine color and anthocyanin composition. *Eur. Food Res. Technol.* **2001**, *213*, 281−285.
(25) Brouillard, R.; Chassaing, S.; Fougerousse, A. Why are grape/fresh wine anthocyanins so simple and why is it that red wine color lasts so long? *Phytochemistry* **2003**, *64*, 1179−1186.
(26) Somers, T. C. The polymeric nature of wine pigments. *Phytochemistry* **1971**, *10*, 2175−2186.
(27) Jurd, L. Review of polyphenol condensation reactions and their possible occurrence in the aging of wines. *Am. J. Enol. Vitic.* **1969**, *20*, 191−195.
(28) Liao, H.; Cai, Y.; Haslam, E. Polyphenol interactions. Anthocyanins: copigmentation and colour changes in red wines. *J. Sci. Food Agric.* **1992**, *59*, 299−305.
(29) Remy, S.; Fulcrand, H.; Labarbe, B.; Cheynier, V.; Moutounet, M. First confirmation in red wine of products resulting from direct anthocyanin-tannin reactions. *J. Sci. Food Agric.* **2000**, *80*, 745−751.
(30) Bakker, J.; Picinelli, A.; Bridle, P. Model wine solutions: colour and composition changes during ageing. *Vitis* **1993**, *32*, 111−118.
(31) Rivas-Gonzalo, J. C.; Bravo-Haro, S.; Santos-Buelga, C. Detection of compounds formed through the reaction of malvidin-3-monoglucoside and catechin in the presence of acetaldehyde. *J. Agric. Food Chem.* **1995**, *43*, 1444−1449.
(32) Timberlake, C. F.; Bridle, P. Interactions between anthocyanins, phenolics compounds and acetaldehyde, and their significance in red wines. *Am. J. Enol. Vitic.* **1976**, *27*, 97−105.
(33) Bakker, J.; Bridle, P.; Honda, T.; Kuwano, H.; Saito, N.; Terahara, N.; Timberlake, C. F. Identification of an anthocyanin occurring in some red wines. *Phytochemistry* **1997**, *44*, 1375−1382.
(34) Bakker, J.; Timberlake, C. F. Isolation, identification, and characterization of new color-stable anthocyanins occurring in some red wines. *J. Agric. Food Chem.* **1997**, *45*, 35−43.
(35) Fulcrand, H.; Benabdeljalil, C.; Rigaud, J.; Cheynier, V.; Moutounet, M. A new class of wine pigments generated by reaction between pyruvic acid and grape anthocyanins. *Phytochemistry* **1998**, *47*, 1401−1407.
(36) Romero, C.; Bakker, J. Interactions between grape anthocyanins and pyruvic acid, with effect of pH and acid concentration on anthocyanin composition and color in model solutions. *J. Agric. Food Chem.* **1999**, *47*, 3130−3139.
(37) Mateus, N.; Silva, A. M. S.; Vercauteren, J.; De Freitas, V. Occurrence of anthocyanin-derived pigments in red wines. *J. Agric. Food Chem.* **2001**, *49*, 4836−4840.
(38) Mateus, N.; De Freitas, V. Evolution and stability of anthocyanin-derived pigments during Port wine aging. *J. Agric. Food Chem.* **2001**, *49*, 5217−5222.
(39) Cameira dos Santos, P. J.; Brillouet, J. M.; Cheynier, V.; Moutounet, M. Detection and partial characterisation of new anthocyanin-derived pigments in wine. *J. Sci. Food Agric.* **1996**, *70*, 204−208.
(40) Fulcrand, H.; Cameira dos Santos, P. J.; Sarni-Manchado, P.; Cheynier, V.; Favre-Bonvin, J. Structure of new anthocyanin-derived wine pigments. *J. Chem. Soc., Perkin Trans.* **1996**, *1*, 735−739.
(41) Schwarz, M.; Wabnitz, T. C.; Winterhalter, P. Pathway leading to the formation of anthocyaninvinylphenol adducts and related pigments in red wines. *J. Agric. Food Chem.* **2003**, *51*, 3682−3687.
(42) Benabdeljalil, C.; Cheynier, V.; Fulcrand, H.; Hakiki, A.; Mosaddak, M.; Moutounet, M. Mise en evidence de nouveaux pigments formes par reaction des anthocyanes avec des metabolites de levures. *Sci. Aliments.* **2000**, *20*, 203−220.
(43) Lu, Y.; Foo, L. Y. Unusual anthocyanin reaction with acetone leading to pyranoanthocyanin formation. *Tetrahedron Lett.* **2001**, *42*, 1371−1373.
(44) Hayasaka, Y.; Asenstorfer, R. E. Screening for potential pigments derived from anthocyanins in red wine using nanoelectrospray tandem mass spectrometry. *J. Agric. Food Chem.* **2002**, *50*, 756−761.
(45) Von Baer, D.; Rentzsch, M.; Hitschfeld, M. A.; Mardones, C.; Vergara, C.; Winterhalter, P. Relevance of chromatographic efficiency in varietal authenticity verification of red wines based on their anthocyanin profiles: Interference of pyranoanthocyanins formed during wine ageing. *Anal. Chim. Acta* **2008**, *621*, 52−56.
(46) De Freitas, V.; Mateus, N. Formation of pyranoanthocyanins in red wines: A new and diverse class of anthocyanin derivatives. *Anal. Bioanal. Chem.* **2011**, *401*, 1463−1473.
(47) Rentzsch, M.; Schwarz, M.; Winterhalter, P. Pyranoanthocyanins-An overview on structures, occurrence, and pathways of formation. *Trends Food Sci. Technol.* **2007**, *18*, 526−534.
(48) Ribéreau-Gayon, P.; Glories, Y.; Maujean, A.; Dubourdieu, D. In *Handbook of Enology Vol. 2 The Chemistry of Wine Stabilization and Treatments*, second ed.; John Wiley & Sons, Ltd.: Chichester, UK, 2005; pp 141−204.
(49) He, J.; Oliveira, J.; Silva, A. M. S.; Mateus, N.; De Freitas, V. Oxovitisins: A new class of neutral pyranone-anthocyanin derivatives in red wines. *J. Agric. Food. Chem.* **2010**, *58*, 8814−8819.
(50) Wright, J. S.; Johnson, E. R.; Di Labio, G. A. Predicting the activity of phenolic antioxidants: theoretical method, analysis of substituent effects and application to major families of antioxidants. *J. Am. Chem. Soc.* **2001**, *123*, 1173−1183.
(51) Leopoldini, M.; Prieto Pitarch, I.; Russo, N.; Toscano, M. Structure, conformation and electronic properties of apigenin, luteolin and taxifolin antioxidants. A first principle theoretical study. *J. Phys. Chem. B* **2004**, *108*, 92−94.
(52) Leopoldini, M.; Marino, T.; Russo, N.; Toscano, M. Antioxidant properties of phenolic compounds. H-atom versus electron transfer mechanism. *J. Phys. Chem. B* **2004**, *108*, 4916−4922.

(53) Leopoldini, M.; Marino, T.; Russo, N.; Toscano, M. Density functional computations of the energetic and spectroscopic parameters of quercetin and its radicals in the gas phase and in solvent. *Theor. Chem. Acc.* **2004**, *111*, 210−216.
(54) Leopoldini, M.; Russo, N.; Chiodo, S.; Toscano, M. Iron Chelation by the Powerful Antioxidant Flavonoid Quercetin. *J. Agric. Food Chem.* **2006**, *54*, 6343−6351.
(55) Chimenti, F.; Cottiglia, F.; Bonsignore, L.; Casu, L.; Casu, M.; Floris, C.; Secci, D.; Bolasco, A.; Chimenti, P.; Granese, A.; Befani, O.; Turini, P.; Alcaro, S.; Ortuso, F.; Trombetta, G.; Loizzo, A.; Guarino, I. Quercetin as the active principle of Hypericum hircinum exerts a selective inhibitory activity against MAO-A: extraction, biological analysis, and computational study. *J. Nat. Prod.* **2006**, *69*, 945−949.
(56) Cornard, J. P.; Dangleterre, L.; Lapouge, C. Computational and characterization of the molecular and electronic structure of the Pb(II)-quercetin complex. *J. Phys. Chem. A.* **2005**, *109*, 10044−10051.
(57) Cornard, J. P.; Merlin, J. C. Spectroscopic and structural study of complexes of quercetin with Al(III). *J. Inorg. Biochem.* **2002**, *92*, 19−27.
(58) Fiorucci, S.; Golebiowski, J.; Cabrol-Bass, D.; Antonczak, S. DFT Study of Quercetin Activated Forms Involved in Antiradical, Antioxidant, and Prooxidant Biological Processes. *J. Agric. Food Chem.* **2007**, *55*, 903−911.
(59) Krishnan, K.; Binkley, J. S.; Seeger, R.; Pople, J. A. Self-consistent molecular orbital methods. XX. A basis set for correlated wave functions. *J. Chem. Phys.* **1980**, *72*, 650−654.
(60) *Jaguar*, version 7.9; Schrödinger, LLC: New York, 2012.
(61) *MacroModel*, version 9.8; Schrödinger, LLC: New York, 2010.
(62) Mohamadi, F.; Richard, N. G. J.; Guida, W. C.; Liskamp, R.; Lipton, M.; Caufield, C.; Chang, G.; Hendrickson, T.; Still, W. C. MacroModel - an Integrated Software System for Modeling Organic and Bioorganic Molecules Using Molecular Mechanics. *J. Comput. Chem.* **1990**, *11*, 440−467.
(63) Jorgensen, W. L.; Tirado-Rives, J. The OPLS Potential Functions for Proteins. Energy Minimization for Crystals of Cyclic Peptides and Crambin. *J. Am. Chem. Soc.* **1988**, *110*, 1657−1666.
(64) Still, W. C.; Tempczyk, A.; Hawley, R. C.; Hendrickson, T. Semianalytical treatment of solvation for molecular mechanics and dynamics. *J. Am. Chem. Soc.* **1990**, *112*, 6127−6129.
(65) Daura, X.; Gademann, K.; Jaun, B.; Seebach, D.; Van Gunsteren, W. F.; Mark, A. E. Peptide folding: When simulation meets experiment. *Angew. Chem. Int.* **1999**, *38*, 236−240.
(66) Tannor, D. J.; Marten, B.; Murphy, R.; Friesner, R. A.; Sitkoff, D.; Nicholls, A.; Ringnalda, M.; Goddard, W. A., III; Honig, B. Accurate First Principles Calculation of Molecular Charge Distributions and Solvation Energies from Ab Initio Quantum Mechanics and Continuum Dielectric Theory. *J. Am. Chem. Soc.* **1994**, *116*, 11875−11882.
(67) Marten, B.; Kim, K.; Cortis, C.; Friesner, R. A.; Murphy, R. B.; Ringnalda, M. N.; Sitkoff, D.; Honig, B. New Model for Calculation of Solvation Free Energies: Correction of Self-Consistent Reaction Field Continuum Dielectric Theory for Short-Range Hydrogen-Bonding Effects. *J. Phys. Chem.* **1996**, *100*, 11775−11788.
(68) Glendening, E. D.; Badenhoop, J. K.; Reed, A. E.; Carpenter, J. E.; Bohmann, J. A.; Morales, C. M.; Weinhold, F. *NBO 5.0*; Theoretical Chemistry Institute, University of Wisconsin: Madison, WI, 2001.
(69) Raczyńska, E. D.; Hallman, M.; Kolczyńska, K.; Stępniewski, T. M. On the Harmonic Oscillator Model of Electron Delocalization (HOMED) Index and its Application to Heteroatomic π-Electron Systems. *Symmetry* **2010**, *2*, 1485−1509.
(70) Leopoldini, M.; Rondinelli, F.; Russo, N.; Toscano, M. yranoanthocyanins: A Theoretical Investigation on Their Antioxidant Activity. *J. Agric. Food Chem.* **2010**, *58*, 8862−8871.
(71) Leopoldini, M.; Russo, N.; Toscano, M. Gas and Liquid Phase Acidity of Natural Antioxidants. *J. Agric. Food Chem.* **2006**, *54*, 3078−3085.
(72) Kabanda, M. M. Antioxidant Activity of Rooperol Investigated through Cu (I and II) Chelation Ability and the Hydrogen Transfer Mechanism: A DFT Study. *Chem. Res. Toxicol.* **2012**, *25*, 2153−2166.